International Journal of Multimedia and Ubiquitous Engineering
Vol.11, No.3 (2016), pp.81-92
http://dx.doi.org/10.14257/ijmue.2016.11.3.08

Discrete Poisson Noise Logging Image Repair Based on Schatten Matrix Operator

Zhang Jian[1,2*], Yang Jie[2] and Zhang bin[2]

1. College of Computer science, Yangtze University, HuBei Jing Zhou, 434023 China
2. Information Engineering School, Wuhan University of Technology, HuBei WuHan, 430070 China
E-mail

Abstract

In order to solve the problem that the present logging image reconstruction algorithm has certain staircase effect and ring effect during the discrete Poisson noise image repair process, a noise reduction algorithm based on Schatten matrix operator for discrete Poisson logging image is proposed in this article. Specifically, Schatten norm matrix of Hessian operator is adopted to estimate each pixel value of the image, and meanwhile the non-quadratic regularization function is adopted to eliminate the staircase effect; then Poisson measurement model is integrated with Schatten regularization function to construct the minimum objective function; then norm proximal mapping estimation algorithm is defined and is adopted to decouple the data fidelity item and the regularization matrix in the objective function, thus to recover the image. The simulation result shows: compared with present denoising technology, the algorithm proposed in this article has better repair effect and greater similarity in the aspect of processing the discrete Poisson noise.

Keywords: *Poisson noise; Schatten standardization; Regularization; Image reconstruction; Hessian operator*

1. Introduction

During the photosensitive detection process of many imaging devices, the image quality can be seriously influenced due to Poisson noise caused by the fluctuation of the detected photons [1-3], especially Poisson noise inverse problem [4-5]. Therefore, many scholars have proposed corresponding Poisson noise reduction algorithms [6-7]. For example, Dupe [8], *et al*. have firstly converted Poisson data into the data able to be processed by Gaussian function through variance stability conversion and then minimized the objective function composed of linear data fidelity item and regularization matrix, thus to realize image reconstruction, and the simulation data display algorithm has better repair effect; Bai Jian [9] has designed a Poisson denoising algorithm based on integral differential equation to eliminate Poisson noise, wherein this equation can effectively eliminate Poisson noise through suitable dimension function, and finally he has also given relevant instances to prove algorithm effectiveness.

These algorithms aims at converting Poisson noise into Gaussian function for image repair and have certain repair effect for Poisson image, but it is difficult for these algorithm to process discrete Poisson images and these algorithms also have obvious blurring effect and staircase effect. Therefore, Schatten norm regularization Poisson logging image reconstruction algorithm based on Hessian operator is proposed in this article. Specifically, Schatten norm matrix and non-quadratic regularization function are adopted to eliminate ring effect and staircase effect; ADMM is adopted and S_p norm

ISSN: 1975-0080 IJMUE

proximal mapping estimation algorithm is defined, thus to decouple the data fidelity item and the regularization matrix in the objective function. Finally, the algorithm reconstruction performance is also tested in this article.

2. Degradation Model

According to linear operator degradation and Poisson noise image, the following degradation model is obtained:

$$y = T(Kx), \tag{1}$$

Therein, matrix K $\in$ RM×N denotes the space response model of the image sensor; T denotes the function for describing the property of the measured noise; $y \in R_+^M$ and $\mathrm{x} \in \mathrm{R}_+^N$ respectively denote the vectorized logging image and the estimated image; R_+ denotes a group of nonnegative real numbers.

3. Matrix Operator Regularization

3.1. S_p Norm Matrix

Firstly, define a group of unitary matrixes $E^n = \{\mathrm{X} \in C^{n\times n} : \mathrm{X}^{-1} = X^H\}$, wherein C is a group of complex numbers and $(.)^H$ is Hermitian transposed matrix.

Then, define a group of positive semi definite diagonal matrixes:

$$W^{n_1\times n_2} = \{X \in R_+^{n_1\times n_2} : X(i,j) = 0 \forall i \neq j\} \tag{1}$$

If X ($X \in C^{n_1\times n_2}$) is set as $X = U\Sigma V^H$ which can be decomposed by a singular value, wherein $U \in E^{n_1}, V \in E^{n_2}$, $\Sigma \in W^{n_1\times n_2}$, then the p -order Schatten norm (S_p normal) can be defined as follows:

$$\|X\|s_p = \left(\sum_{k=1}^{\min(n_1,n_2)} \sigma_k^p\right)^{\frac{1}{p}} \tag{2}$$

Therein, $p \geq 1$; p denotes the order of S_p norm; σ_k denotes the Kth singular value of X.

3.2. Regularization of Hessian Operator and Matrix Operator

The discrete Hessian operator is denoted by H, and the image intensity in $N_x \times N_y$ grid is assumed to be rasterized by vector x with the dimensionality as $N = N_x . N_y$ in order to make the pixel at the coordinate (i, j) mapped to the nth entry of vector x, wherein the mapping relation can be expressed as $n = jN_x + (i+1)$. Then, the discrete Hessian operator shall meet the mapping relation $\mathrm{H} : : R^n \mapsto g$ ($g = R^{n\times 2\times 2}$). For $\mathrm{x} \in R^n$, $\mathrm{H_x}$ can be defined as follows:

$$[\mathrm{H_x}]_n = \begin{bmatrix} [\Delta_{r1r1}X]_n & [\Delta_{r1r2}X]_n \\ [\Delta_{r1r2}X]_n & [\Delta_{r2r2}X]_n \end{bmatrix} \tag{3}$$

Therein, $n = 1,..., N$; $\Delta_{r1r1}, \Delta_{r2r2}, \Delta_{r1r2}$ denotes the finite difference operator.

Then, Hessian operator and S_p norm can be combined to obtain the regularized Hessian Schatten norm matrix operator:

$$\mathrm{H}s_p(\mathrm{x}) = \left\|\mathrm{H}_\mathrm{x}\right\|_1, p = \sum_{n=1}^{N} \left\|\left[\mathrm{H}_\mathrm{x}\right]_n\right\| S_p, \forall p \geq 1 \tag{4}$$

4. Poisson Image Reconstruction Algorithm Design

Poisson image reconstruction in this article includes two parts: 1. Obtain punishment ML estimation value; 2. Decouple data fidelity item and regularization matrix.

4.1. Punishment ML Estimation Value

According to Model (1) and Model (4), punishment ML estimation value $\hat{x}$ of an image can be obtained:

$$\begin{aligned} \hat{x} = \arg\min_{\mathrm{x}\in R^N} \Big(& f(\mathrm{x}) = \sum_{m=1}^{M} \left([K\mathrm{x}]_m - y_m \log [K\mathrm{x}]_m \right) \\ & + \tau \left\|\mathrm{H}_\mathrm{x}\right\|_1, p + \iota C(\mathrm{x}) \Big) \end{aligned} \tag{5}$$

Therein, $\tau \geq 0$ is the regularization parameter used to balance data fidelity and punishment item; ιC is the indicator function of convex set $C \in R_+^N$.

Then, Model (5) is evolved into a general form:

$$\hat{x} = \arg\min_{\mathrm{x}\in R^N} \left(\sum_{k=1}^{K} f_k(A_k \mathrm{x}) \right) \tag{6}$$

Therein, A_k is a linear operator in mapping relation $A_k : R^N \mapsto X_k$.

In order to rapidly find solution $\hat{x}$, ADMM is introduced in this article to decouple (6) [10]. If auxiliary variable $Z_k = A_k \mathrm{x} \in X_k$ is introduced, then Model (6) can be converted as follows:

$$\begin{aligned} \min_{\substack{\mathrm{x}\in \mathrm{R}^N \\ Z = A\mathrm{x}\in \mathrm{X}}} \quad & f(Z) = \sum_{k=1}^{K} f_k(Z_k) \end{aligned} \tag{7}$$

Therein, $Z = A\mathrm{x}$ denotes the mapping of x in a multiple linear space $X = X_1 \times \ldots \times X_k$, and the following formula can be obtained:

$$Z = \begin{bmatrix} Z_1 \\ \vdots \\ Z_k \end{bmatrix} = \begin{bmatrix} A_1 \mathrm{x} \\ \vdots \\ \mathrm{A_k x} \end{bmatrix} = A\mathrm{x} \tag{8}$$

The general form of ADMM is as follows:

$$\min_{Ax+Bz=c} g(\mathrm{x}) + f(z) \tag{9}$$

Therein, $\mathrm{x} \in \mathrm{R}^N, z \in R^M, A \in R^{L\times N}, B \in R^{L\times M}, c \in R^L$.

The augmented Lagrange equation corresponding to Formula (7) is as follows:

$$\mathcal{L}_a(x, z, \lambda) = f(z) + \langle \lambda, Ax - z \rangle X + \frac{a}{2} \|Ax - z\|_X^2 \tag{10}$$

Therein, $\lambda \in X$ is corresponding to dual variable $\lambda_k \in X_k$ and $a > 0$ is a penalty parameter; $\langle .,. \rangle_X$ and $\|.\|_X$ respectively denote internal product and standard linear space X. ADMM iterative formula corresponding to Formula (7) is as follows:

$$z^{t+1} = \underset{z \in X}{\operatorname{argmin}} \; f(z) + \frac{a}{2}\left\| z - \left(A\mathrm{x}^{\mathrm{t}} + s^{t} \right) \right\|_{X}^{2} \tag{11a}$$

$$\mathrm{x}^{t+1} = \underset{\mathrm{x} \in R^{n}}{\operatorname{argmin}} \left\| A\mathrm{x} - \left(z^{\mathrm{t}+1} - s^{t} \right) \right\|_{X}^{2} \tag{11b}$$

$$s^{t+1} = s^{t} + A\mathrm{x}^{\mathrm{t}+1} - z^{t+1} \tag{11c}$$

Therein, $s = \frac{\lambda}{a}$.

z-update in ADMM is decoupled by K element to obtain the following formula:

$$\begin{aligned} & f(z) + \frac{a}{2}\left\| z - \left(A\mathrm{x}^{\mathrm{t}} + s^{t} \right) \right\|_{X}^{2} \\ & = \sum_{k=1}^{K} f_{k}(z_{k}) + \frac{a}{2}\left\| z_{k} - \left(A_{k}\mathrm{x}^{\mathrm{t}} + s_{k}^{t} \right) \right\|_{X_{k}}^{2} \end{aligned} \tag{12}$$

Through Model (11a), each z_{k}^{t+1} can be independently converted as follows for relevant calculation:

$$z_{k}^{t+1} = \mathrm{prox}_{f_{k/a}}(\mathrm{u}_{\mathrm{k}}^{\mathrm{t}}), \forall k = 1,...,k, \tag{13}$$

Therein, $\mathrm{u}_{\mathrm{k}}^{\mathrm{t}} = A_{k}\mathrm{x}^{\mathrm{t}} + s_{k}^{t} \in X_{k}$.

4.2. Decoupling of Data Fidelity Item and Regularization Matrix

Finally, objective function $f(x)$ is decoupled, and (5) is converted as follows:

$$\min_{\substack{x \in R^{N} \\ z_{k} = A_{k}x \in X_{k}, k=1,...,3}} \; f_{1}(Z_{1}) + f_{2}(Z_{2}) + f_{3}(Z_{3}) \tag{14}$$

Therein, $A_{1} = K, A_{2} = \mathrm{H}, A_{3} = I$.

$$\begin{cases} f_{1}(Z_{1}) = \sum_{m=1}^{M}\left(\left[Z_{1} \right]_{m} - y_{m} \log\left[Z_{1} \right]_{m} \right) \\ f_{2}(Z_{2}) = \tau \left\| Z_{2} \right\|_{1}, p \\ f_{3}(Z_{3}) = \iota C(Z_{3}) \end{cases} \tag{15}$$

Therefore, the approximate mapping $\mathrm{prox}_{f_{1/a}}\left(\mathrm{u}_{1}^{\mathrm{t}} \right)$ of $\mathrm{u}_{1}^{\mathrm{t}} = K\mathrm{x}^{\mathrm{t}} + \mathrm{s}_{1}^{\mathrm{t}}$ is as follows:

$$\mathrm{z}_{1}^{\mathrm{t}+1} = \frac{1}{2}\left(\mathrm{u}_{1}^{\mathrm{t}} - \frac{1}{a} + \sqrt{\left(\mathrm{u}_{1}^{\mathrm{t}} - \frac{1}{a} \right)^{2} + \frac{4y}{a}} \right) \tag{16}$$

Additionally, f_{3} refers to the indicator function, its approximate mapping is corresponding to its projection in convex set C. The projection formula is as follows:

$$\mathrm{prox}_{f\,3/\mathrm{a}}\left(\mathrm{u}_{3}^{\mathrm{t}} \right) = \max\left(\mathrm{u}_{3}^{\mathrm{t}}, 0 \right) \tag{17}$$

Therein, $\mathrm{u}_{3}^{\mathrm{t}} = \mathrm{x}^{\mathrm{t}} + \mathrm{s}_{3}^{\mathrm{t}}$; $\boldsymbol{0}$ is a zero vector with the dimension as the same as that of $\mathrm{u}_{3}^{\mathrm{t}}$; $\max$ is calculated on the basis of specific components. Finally, in order to obtain z-updates, it is necessary to calculate the approximate mapping related to function f_{2}. According to Model (15), A_{2} is corresponding to Hessian operator, so $Z_{2} \in g$.

Additionally, $\text{prox}_{f_{2/a}}\left(u_2^t\right)$ can be also decomposed through $u_2^t = Hx^t + s_2^t \in g$. Therefore, the following formula can be obtained for variable $Y \in g$:

$$\begin{aligned}\text{prox}_{f_{2/a}}(Y) &= \arg\min_{X \in g} \frac{1}{2}\|X - Y\|_g^2 + \frac{\tau}{a}\|X\|_{1,p} \\ &= \arg\min_{X_n \in R^{2\times 2}} \sum_{n=1}^{N} \frac{1}{2}\|X_n - Y_n\|_F^2 + \frac{\tau}{a}\|X_n\|_{S_p}\end{aligned} \tag{18}$$

On the basis of combining Model (18), the calculation of f_2 approximate mapping can be concluded as the calculation of the approximate mapping of N function, and the function is defined as follows:

$$\text{prox}_{\tau\|.\|S_p}(Y) = \arg\min_{X \in R^{2\times 2}} \frac{1}{2}\|X - Y\|_F^2 + \tau\|X\|_{S_p} \tag{19}$$

In order to effectively execute Model (19), the following proposition is defined in this article:

Proposition 1: set $Y \in C^{n_1 \times n_2}$, wherein Y is matrix $Y = U\Sigma V^H$ which can be decomposed by a singular value; $U \in E^{n_1}$, $V \in E^{n_2}$ and $\Sigma \in W^{n_1 \times n_2}$. If $\Psi_p(.) = \tau\|.\|S_p$ and $\phi_p(.) = \tau\|.\|_p$ are true, then the following approximate mapping can be obtained:

$$\hat{X} = \text{prox}_{\psi_p}(Y) \tag{20}$$

Namely:

$$\hat{X} = U diag\left(\text{prox}_{\varphi_p}(\sigma)\right)V^H \tag{21}$$

Therein, $diag(.)$ is a diagonal matrix and σ denotes a vector of singular value Y.

Argumentation: all Schatten norms are invariable, so the approximate mapping (20) can be equivalent to:

$$\begin{aligned}\hat{X} = \text{prox}_{\psi_p}(Y) &= \arg\min_X \frac{1}{2}\|X - Y\|_F^2 + \tau\|X\|_{S_P} \\ &= \arg\min_X \frac{1}{2}\|U^H XV - U^H YV\|_F^2 + \tau\|U^H XV\|_{S_P}\end{aligned} \tag{22}$$

Matrix $Z = U^H XV$ is put into (22) to obtain:

$$\hat{Z} = \arg\min_Z \underbrace{\frac{1}{2}\|Z - \Sigma\|_F^2 + \tau\|Z\|_{S_P}}_{h(Z;\Sigma)} \tag{23}$$

Proposition 1 can provide the direct relation between the approximate mapping of a ℓ_p vector norm and the approximate mapping of a S_p matrix norm. According to Proposition 1, an algorithm is designed in this article to estimate the approximate mapping of a S_p norm:

(1) Decompose Y through singular vector and singular value mentioned in singular value decomposition method;

(2) Estimate the approximate mapping of ℓ_p norm in σ (a vector of singular value Y);

(3) Adopt the result of Step (2) for reconstruction through the singular value in order to obtain final result.

The optimal solution of (23) is a positive semi-definite diagonal matrix.

$$\begin{aligned} h(\hat{Z};\Sigma) &= \frac{1}{2}\left\|\hat{Z}\right\|_F^2 + \frac{1}{2}\|\Sigma\|_F^2 - \mathrm{Re}\left(tr\left(\hat{Z}^H\Sigma\right)\right) + \tau\left\|\hat{Z}\right\|_{S_p} \\ &\geq \frac{1}{2}\left\|\hat{\Sigma}\right\|_F^2 + \frac{1}{2}\|\Sigma\|_F^2 - tr\left(\hat{\Sigma}^T\Sigma\right) + \tau\left\|\hat{\Sigma}\right\|_{S_p} \\ &= \frac{1}{2}\left\|\hat{\Sigma}-\Sigma\right\|_F^2 + \tau\left\|\hat{\Sigma}\right\|_{S_p} = h(\hat{\Sigma};\Sigma) \end{aligned} \tag{24}$$

Therein, $\hat{\Sigma}$ is a diagonal matrix of singular value $\hat{Z}$. Obviously, the in-equation in (24) shall meet the following condition:

$$\mathrm{Re}\left(tr\left(A^H B\right)\right) \leq \left\langle \sigma_A, \sigma_B \right\rangle_2 \tag{25}$$

Therein, $A, B \in C^{n_1 \times n_2}$; σ_A, σ_B respectively refer to the vectors of singular values A and B. Additionally, the above in-equation can be obtained according to Von Neumann tracking theorem.

According to the result of Schatten norm definition, equation $\left\|\hat{Z}\right\|_{S_p} = \left\|\hat{\Sigma}\right\|_{S_p}, \forall_p \geq 1$ can be obtained.

$\hat{Z}$ is the least element of function h, so $h\left(\hat{Z};\Sigma\right)$ shall be the minimum value. According to Model (24), the lower bound of $h\left(\hat{Z};\Sigma\right)$ can be obtained and meanwhile indicates $h(\hat{Z};\Sigma) = h(\hat{\Sigma};\Sigma)$. Therefore, $\hat{Z} = \hat{\Sigma}$ is true, and $h\left(\hat{Z};\Sigma\right)$ is the minimum value. This also indicates that $\hat{Z}$ is a positive semi-definite diagonal matrix and the optimal solution of Model (23) is also a positive semi-definite diagonal matrix. Additionally, the solution of Model (23) can be expressed as $\hat{Z} = diag\left(\hat{Z}\right)$, wherein $\hat{Z}$ can be obtained according to Formula (26):

$$\hat{Z} = \mathrm{prox}_{\phi_p}(\sigma) = \arg\min_{Z \in R^{\min(n_1,n_2)}} \frac{1}{2}\|Z-\sigma\|_2^2 + \tau\|Z\|_p \tag{26}$$

σ vector can be obtained through diagonal element Σ, and then Model (21) can be obtained through the optimal solutions of Models (22) and (23).

So far, the argumentation is ended.

Finally, x-update of present partition method can be obtained through processing a linear equation system, wherein the linear equation system is as follows:

$$X^{t+1} = \left(K^T K + \mathrm{H}^* \mathrm{H} + \mathrm{I}\right)^{-1}\left(K^T\left(Z_1^{t+1} - S_1^t\right) + \mathrm{H}^*\left(Z_2^{t+1} - S_2^t\right) + \left(Z_3^{t+1} - S_3^t\right)\right) \tag{27}$$

Therein, $\mathrm{H}^*\mathrm{H} = \Delta_{r_1 r_1}^* \Delta_{r_1 r_1} + 2\Delta_{r_1 r_2}^* \Delta_{r_1 r_2} + \Delta_{r_2 r_2}^* \Delta_{r_2 r_2}$.

In Poisson inverse problem, degeneracy operator K does not have any special structure, so the deflection gradient method (DG) can be used to process Formula (27) in order to obtain x-update.

5. Enclosure Form of Approximate Mapping of S_p Norm ($p = 1, 2, \infty$)

According to Proposition 1, the approximate mapping of S_1 norm is correlated to that of ℓ_1 norm, and the approximate mapping of ℓ_1 norm can be obtained through the soft threshold value operator $S_\gamma(\sigma) = \max(\sigma - \gamma, 0)$, wherein γ is a threshold value. Therefore, the approximate mapping of S_1 norm can be obtained:

$$\mathrm{prox}_{\tau\|\cdot\|_{S_1}}(Y) = U diag\left(S_\tau(\sigma)\right)V^H \tag{28}$$

Therein, σ is a vector of singular value Y.

Then, according to Proposition 1 and the approximate mapping of ℓ_2 norm, the approximate mapping of S_2 norm can be obtained. The approximate mapping of ℓ_2 norm is as follows:

$$\text{prox}_f(y) = \arg\min_{X \in Q} \frac{1}{2}\|x-y\|_Q^2 + f(x) \tag{29}$$

Therein, Q is a multiple linear space $Q = Q_1, ...Q_K$.

On the basis of combining Model (29), the approximate mapping of S_2 norm can be obtained:

$$\text{prox}_{\tau\|\cdot\|_{S_2}}(Y) = \begin{cases} W, & \text{if } \|Y\|_{S_2} \le \tau \\ \left(\dfrac{\|Y\|_{S_2}-\tau}{\|Y\|_{S_2}}\right)Y, & \text{if } \|Y\|_{S_2} \ge \tau \end{cases} \tag{30}$$

Therein, W is a zero matrix with the dimension as the same as that of Y, and the calculation of the approximate mapping of S_∞ norm needs the following approximate mapping of ℓ_∞ norm:

$$\text{prox}_{\tau\|\cdot\|_\infty}(\sigma) = \min(\sigma, \tau\gamma.\text{b}) \tag{31}$$

Therein, **b** is a complex vector. For any $\sigma \in R_+^2$, γ can be calculated through decomposition method:

$$\gamma = \begin{cases} 0, & \text{if } \sigma_1 \le 1-\sigma_2 \\ \dfrac{\sigma_1+\sigma_2-1}{2}, & \text{if } 1-\sigma_2 < \sigma_1 \le 1+\sigma_2 \\ \sigma_1-1, & \text{if } \sigma_1 > 1+\sigma_2 \end{cases} \tag{32}$$

Therein, σ_1, σ_2 are respectively the maximum value and the minimum value of σ. The approximate mapping of S_∞ norm is as follows:

$$\text{prox}_{\tau\|\cdot\|_{S_\infty}}(Y) = Udiag(\min(\sigma, \tau\gamma.b))V^H \tag{33}$$

6. Simulation Result and Analysis

In order to verify the validity and the excellence of the algorithm proposed in this article, the contrast algorithms are set as follows: literature [12] is recorded as algorithm A and literature [13] is recorded as algorithm B. Corresponding result is obtained through MATLAB test. Specifically, Figure 1(a) is taken as the actual logging image, and discrete Poisson noise and Gaussian blur are added therein to generate the target to be reconstructed, as shown in Figure 1(b); then the technology proposed in this article and the contrast algorithms are adopted to repair Figure1 (b), and the corresponding results are as shown in Figure 1(c)~Figure 1(e).

6.1. Noise Reduction Effect of Discrete Poisson Logging Image

The results of adopting different denoising technologies to repair Figure 1(b) are as shown in Figure1. According to the visual quality in the following figures, the noise reduction technology proposed in this article has better effect for eliminating Poisson noise, as shown in Figure 1(e), wherein the denoised image does not have any ring effect and the texture edge of the logging image can be well preserved, without any image information loss. However, the contrast denoising algorithms do not have ideal effect; although the results are visually accepted, these contrast algorithms have certain staircase effect and edge blur, as shown in Figure1(c) and Figure1(d). Actually, Schatten norm

matrix of Hessian operator is introduced in this article to estimate each pixel value of the image in order to better adapt to the variation of image intensity. Meanwhile, the non-quadratic regularization function is adopted to take S_p norm regularization matrix as the regularization function of the potential function for solving Poisson inverse problem in order to effectively eliminate staircase effect. However, the contrast algorithms are mainly used to process common noise, without the consideration of discrete Poisson inverse problem, so it is difficult for such algorithms to reconstruct discrete Poisson noise.

(a) Target Image

(b) Discrete Poisson Noise + Gaussian Blur

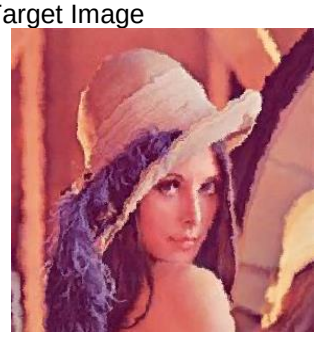

(c) Image Denoised by Algorithm A

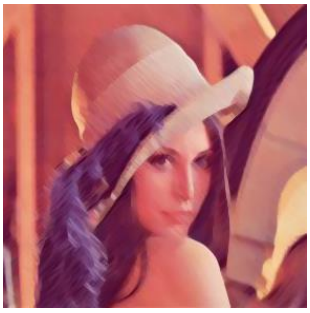

(d) Image Denoised by Algorithm B

(e) Image Denoised by Technology Proposed in this Article

Figure 1. Noise Reduction Effects of Different Denoising Technologies

6.2. Contrastive Analysis of Structure Similarity SSIM

Structure similarity $(SSIM-Structure\ Similarity)$ is an important indicator [14] for evaluating the logging image repair quality, so $SSIM$ is adopted in this article to quantize the denoising effects of these denoising technologies. Before testing $SSIM$ value, it is necessary to adopt fitting approach technology to obtain the curves of the predicted value and the subjective value of the test object. In this article, the test is carried out in $USC-SIPI$ dataset to obtain $DMOS$ ($Difference\ of\ Mean\ Optinion\ Score$) and $SSIM$ curves, as shown in Figure2. The specific steps are as follows: firstly, the three noise reduction algorithms are adopted to repair the image in Figure3(b), wherein the corresponding output results are as

shown in Figure3(c) ~ Figure3(e); then, obtain *DMOS* values of Figure3(c) ~ Figure3(e) corresponding to Figure3(a) according to the method mentioned in literature [16]. According to Figure2, *SSIM* of each algorithm can be finally obtained, as shown in Table 1. According to Figure3 and Table 1, the algorithm proposed in this article has optimal noise reduction effect and the output logging image has clear texture edge, without any ring effect and staircase effect, thus to make the algorithm proposed in this article have small distortion degree and maximum *SSIM* value, namely 0.927. Additionally, the image reconstructed by algorithm A has obvious ring effect, as shown in Figure3(c), and the output image losses texture and edge (the characters in the image are blurry); the image reconstructed by algorithm B is blurry and partially losses the texture; *SSIM* values of algorithms A and B are respectively 0.826 and 0.904. If *SSIM* value is larger, then it is indicated that the denoised image is more similar with the image in Figure2(a), because Schatten norm matrix of Hessian operator is introduced into the algorithm proposed in this article to better adapt to the variation of image intensity, and meanwhile the non-quadratic regularization function is also adopted to eliminate staircase effect and enable the repaired image to have least texture edge loss as well as maximally preserve image information, thus to have minimum distortion and maximum *SSIM* value. However, it is difficult for the contrast algorithms to process discrete Poisson noise, so the reconstructed image has large distortion and accordingly has minimum *SSIM* value. Therefore, the noise reduction technology proposed in this article can effectively process discrete Poisson noise.

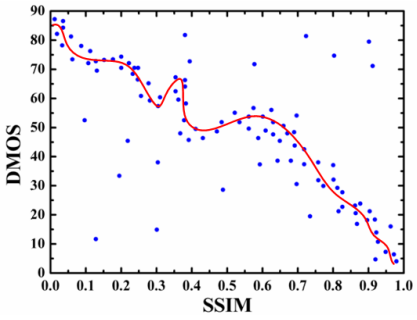

Figure 2. Fitting Curve of *DMOS* and *SSIM*

(a) Target Image

(b) Discrete Poisson Noise + Gaussian Blur

(c) Image Denoised by Algorithm A (d) Image Denoised by Algorithm B

(d) Image Denoised by Technology Proposed in this Article

Figure 3. Noise Reduction Effect of Different Denoising Technologies

Table 1. Average *PSNR* Corresponding to Different Algorithms

Name	Algorithm Proposed in this Article	Algorithm A	Algorithm B
(dB) Average PSNR (dB)	0.927	0.826	0.904

7. Conclusion

In order to solve the difficulty in using the present noise reduction algorithm for processing Poisson noise, a Poisson logging image reconstruction algorithm based on matrix value operator is proposed in this article. Specifically, Schatten norm matrix of Hessian operator is introduced therein to estimate each pixel of the image in order to make the algorithm widely applicable to natural images; the non-quadratic regularization function is also adopted to eliminate staircase effect; Poisson measurement model and Hessian Schatten regularization model are combined to construct the minimum objective function; ADMM is adopted to decouple the data fidelity item and the regularization matrix in the objective function and denoise the image. The experimental data show: compared with present image denoising technology, this denoising technology has better quality and can significantly reduce staircase effect and ring effect.

Acknowledgement

This work was supported by the National Natural Science Foundation of China under Grant No. 41374148, and Educational Commission of Hubei Province of China under Grant No. Q20111306.

References

[1] T. Su, W. Wang, Z. Lv, W. Wu and X. Li, "Rapid Delaunay Triangulation for Random Distributed Point Cloud Data Using Adaptive Hilbert Curve", Computers & Graphics, **(2015)**.
[2] J. Hu, Z. Gao and W. Pan, "Multi-angle Social Network Recommendation Algorithms and Similarity Network Evaluation", Journal of Applied Mathematics, vol. 2013, **(2013)**.
[3] Z. Lv, T. Yin, Y. Han, Y. Chen and G. Chen, "WebVR——web virtual reality engine based on P2P network", Journal of Networks, vol. 6, no. 7, **(2011)**, pp. 990-998.
[4] J. Yang, B. Chen, J. Zhou and Z. Lv, "A portable biomedical device for respiratory monitoring with a stable power source", Sensors, **(2015)**.
[5] G. Liu, Y. Geng and K. Pahlavan, "Effects of calibration RFID tags on performance of inertial navigation in indoor environment", 2015 International Conference on Computing, Networking and Communications (ICNC), **(2015)**.
[6] J. He, Y. Geng, Y. Wan, S. Li and K. Pahlavan, "A cyber physical test-bed for virtualization of RF access environment for body sensor network", IEEE Sensor Journal, vol. 13, no. 10, **(2013)**, pp. 3826-3836.
[7] W. Huang and Y. Geng, "Identification Method of Attack Path Based on Immune Intrusion Detection", Journal of Networks, vol. 9, no. 4, **(2014)**, pp. 964-971.
[8] Z. Lv, C. Esteve, J. Chirivella and P. Gagliardo, "Clinical Feedback and Technology Selection of Game Based Dysphonic Rehabilitation Tool", 2015 9th International Conference on Pervasive Computing Technologies for Healthcare (PervasiveHealth2015), IEEE, **(2015)**.
[9] W. Ke, "Next generation job management systems for extreme-scale ensemble computing", Proceedings of the 23rd international symposium on High-performance parallel and distributed computing. ACM, **(2014)**.
[10] L. Tonglin, "Distributed Key-Value Store on HPC and Cloud Systems", 2nd Greater Chicago Area System Research Workshop (GCASR), **(2013)**.
[11] Y. Su, "In-situ bitmaps generation and efficient data analysis based on bitmaps", In Proceedings of the 24th International Symposium on High-Performance Parallel and Distributed Computing, ACM, **(2015)**, pp. 61-72.
[12] G. Yan, Y. Lv, Q. Wang and Y. Geng, "Routing algorithm based on delay rate in wireless cognitive radio network", Journal of Networks, vol. 9, no. 4, **(2014)**, pp. 948-955.
[13] D. Jiang, X. Ying, Y. Han and Z. Lv, "Collaborative Multi-hop Routing in Cognitive Wireless Networks", Wireless Personal Communications, **(2015)**.
[14] G. Bao, L. Mi, Y. Geng and K. Pahlavan, "A computer vision based speed estimation technique for localizing the wireless capsule endoscope inside small intestine", 36th Annual International Conference of the IEEE Engineering in Medicine and Biology Society (EMBC), **(2014)**.
[15] W. Gu, Z. Lv and M. Hao, "Change detection method for remote sensing images based on an improved Markov random field", Multimedia Tools and Applications, **(2016)**.
[16] Y. Geng and K. Pahlavan, "On the accuracy of rf and image processing based hybrid localization for wireless capsule endoscopy", IEEE Wireless Communications and Networking Conference (WCNC), **(2015)**.
[17] Z. Xiaobing, "Exploring Distributed Resource Allocation Techniques in the SLURM Job Management System", Illinois Institute of Technology, Department of Computer Science, Technical Report, **(2013)**.
[18] G. Bao, L. Mi, Y. Geng, M. Zhou and K. Pahlavan, "A video-based speed estimation technique for localizing the wireless capsule endoscope inside gastrointestinal tract", 2014 36th Annual International Conference of the IEEE Engineering in Medicine and Biology Society (EMBC), **(2014)**.
[19] D. Zeng and Y. Geng, "Content distribution mechanism in mobile P2P network", Journal of Networks, vol. 9, no. 5, **(2014)**, pp. 1229-1236.
[20] Z. Lu, C. Esteve, J. Chirivella and P. Gagliardo, "A Game Based Assistive Tool for Rehabilitation of Dysphonic Patients", 3rd International Workshop on Virtual and Augmented Assistive Technology (VAAT) at IEEE Virtual Reality 2015 (VR2015), Arles, France, IEEE, **(2015)**.
[21] J. He, Y. Geng and K. Pahlavan, "Toward Accurate Human Tracking: Modeling Time-of-Arrival for Wireless Wearable Sensors in Multipath Environment", IEEE Sensor Journal, vol. 14, no. 11, **(2014)**, pp. 3996-4006.
[22] W. Ou, Z. Lv and Z. Xie, "Spatially Regularized Latent topic Model for Simultaneous object discovery and segmentation", The 2015 IEEE International Conference on Systems, Man, and Cybernetics (SMC), **(2015)**.
[23] W. Wang, Z. Lu, X. Li, W. Xu, B. Zhang and X. Zhang, "Virtual Reality Based GIS Analysis Platform", 22th International Conference on Neural Information Processing (ICONIP), Istanbul, Turkey, **(2015)**.
[24] W. Ke, "Using Simulation to Explore Distributed Key-Value Stores for Exascale System Services", 2nd Greater Chicago Area System Research Workshop (GCASR), **(2013)**.
[25] J. He, Y. Geng, F. Liu and C. Xu, "CC-KF: Enhanced TOA Performance in Multipath and NLOS Indoor Extreme Environment", IEEE Sensor Journal, vol. 14, no. 11, **(2014)**, pp. 3766-3774.
[26] S. Zhou, L. Mi, H. Chen and Y. Geng, "Building detection in Digital surface model", 2013 IEEE International Conference on Imaging Systems and Techniques (IST), **(2012)**.

[27] N. Lu, C. Lu, Z. Yang and Y. Geng, "Modeling Framework for Mining Lifecycle Management", Journal of Networks, vol. 9, no. 3, **(2014)**, pp. 719-725.
[28] L. Tonglin, "ZHT: A light-weight reliable persistent dynamic scalable zero-hop distributed hash table", Parallel & Distributed Processing (IPDPS), 2013 IEEE 27th International Symposium on. IEEE, **(2013)**.
[29] W. Ke, "Optimizing load balancing and data-locality with data-aware scheduling." Big Data (Big Data)", 2014 IEEE International Conference on. IEEE, **(2014)**.

Author

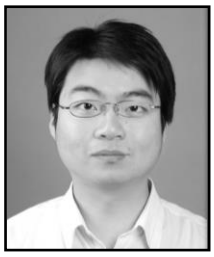

Zhang Jian, received his M.S. degree in technology of Computer application from Yangtze University in HuBei, China. He is currently a lecturer in the School of Computer Science and technology at Yangtze University. His research interest is mainly in the area of Ultrasound logging image processing, Signal Detection and Control. He has published several research papers in scholarly journals in the above research areas and has participated in several books.

